PHOTOGRAMMETRIC MONITORING OF AN ARTIFICIALLY GENERATED SHALLOW LANDSLIDE

DEVRIM AKCA (akca@isikun.edu.tr)
Isik University, Istanbul, Turkey

Formerly at Swiss Federal Institute of Technology (ETH), Zurich

(Extended version of a paper presented at the International Conference on GeoInformation for Disaster Management (Gi4DM'11), held in Antalya from 3rd to 8th May 2011)

Abstract

An artificial rainfall event was applied to a forested slope in Ruedlingen, northern Switzerland. The experiment triggered a landslide which resulted in mobilising about 130 m³ of debris. The event was monitored by a photogrammetric camera network in order to quantify spatial and temporal changes. A 4-camera arrangement was used for the image acquisition. The cameras operated at a data acquisition rate of 5 to 8 frames per second (fps) on average. The surface deformation was quantified by tracking the small (tennis) balls pegged into the ground. Image measurements were performed using the automated image matching methods, which was implemented in an in-house developed software package. 3D coordinates of the target points were estimated by running a customized type of bundle adjustment in batch computation mode. The average 3D point positioning precision of ±1·8 cm was achieved.

KEYWORDS: close range photogrammetry, landslide monitoring, high speed camera, network design, photogrammetric network simulation, camera synchronisation, point tracking, bundle adjustment

INTRODUCTION

THE UNDERSTANDING OF LANDSLIDE mechanisms is greatly facilitated when information on their horizontal and vertical displacements is available (Dewitte et al., 2008). Geotechnical sensors, such as piezometers, inclinometers, and extensometers have been used in great extend (Angeli et al., 2000; Ayalew et al., 2005; Corsini et al., 2005), although they only provide 1D information.

Geodetic techniques can provide 2D and even 3D spatial information in point or surface forms. Remote sensing satellite imageries (Metternicht et al., 2005; Martha et al., 2010; Lodhi, 2011; Debella-Gilo and Kääb, 2012), Global Positioning Systems (Malet et al., 2002; Mora et al., 2003), motorized theodolites and electromagnetic distance meters (Petley et al., 2005), ground-based SAR interferometry (Tarchi et al., 2003), terrestrial laser scanning (Travelletti et al., 2008; Pesci et al., 2011), unmanned aerial vehicles (Niethammer et al., 2012), airborne photogrammetry (Chadwick et al., 2005; Dewitte et al., 2008; Baldi et al., 2008), airborne laser scanning (Bell et al., 2012) and high speed digital cameras (Dewez et al., 2010) have been utilized for the pre- and post-analysis of landslide events, risk assessment and long term monitoring tasks.

The event of landslide must be monitored by a measurement system operating at a very high data acquisition rate when thorough understanding of landslide dynamics is researched. Digital close range photogrammetry is an optimal solution for such missions in terms of data frequency, coverage, resolution and accuracy. Ochiai et al. (2004) monitored an artificial rainfall induced landslide using close range photogrammetry. They have determined motion of the surface using the five stereo pairs of ten low resolution (640×480 pixels) CCD cameras.

TRAMM (Triggering of Rapid Mass Movements in Steep Terrain) is an inter-disciplinary project conducted in cooperation of Swiss Federal Research Institute WSL, ETH Zurich, and EPF Lausanne. The primary goal of the project is to improve the quantification and predictability of hazardous mass movements including landslides, snow avalanches, and debris flows. The project aims to conduct laboratory and field experiments, spatial analyses of hill-slope failures, development of new modelling approaches and new measurement methodologies. The following research tasks are emphasized: spatial characterization of hazard prone slopes, improved understanding of triggering mechanisms and mass dynamics.

The TRAMM project has six test sites. An artificial shallow landslide was generated at one of them near a small town in the north of Switzerland, Ruedlingen, and the mass dynamics were studied numerically. Parameters such as pore water pressure, volumetric water content, horizontal soil pressure, temperature, piezometric water level, surface and subsurface deformations were monitored during the sprinkling experiment (Askarinejad et al., 2010; Springman, et al., 2010).

This paper covers the details of the (close range) photogrammetric image data processing work of the Ruedlingen experiment. The goal of the photogrammetric work is to quantify spatial and temporal changes of the landslide surface. Points were signalized with markers and their movement was tracked during the landslide, while their 3D coordinates were estimated at each instant of the image acquisition frequency. The photogrammetric work provides input of the geotechnical analysis for better understanding of the landslide characteristics, and also provides external data for validation of other field instruments.

The first sprinkling experiment was conducted in autumn 2008 in which the failure had not occurred. Subsequently, the second experiment was planned and executed in spring 2009 which was resulted in a landslide. In the previous publication (Akca et al., 2011), characterization of the test site, the workflow and

the numerical results of both of the sprinkling experiments were covered. This paper focuses on the second experiment. The computational and algorithmic details of the photogrammetric work are emphasized.

The next chapter introduces the test site area. The third chapter elaborates the experiment. The photogrammetric network design, network simulation, equipments and installation, camera calibration, image orientation, target tracking and point positioning with bundle adjustment aspects are explained in detail.

TEST SITE IN RUEDLINGEN

The test site is located on a steep slope next to the River Rhine in Ruedlingen, a small town in the north of Switzerland (Fig. 1). The test area is about 10 m by 35 m in size and has an average slope of 38 degrees (Fig. 2). The ground was cleared from trees and bushes prior to the experiment.
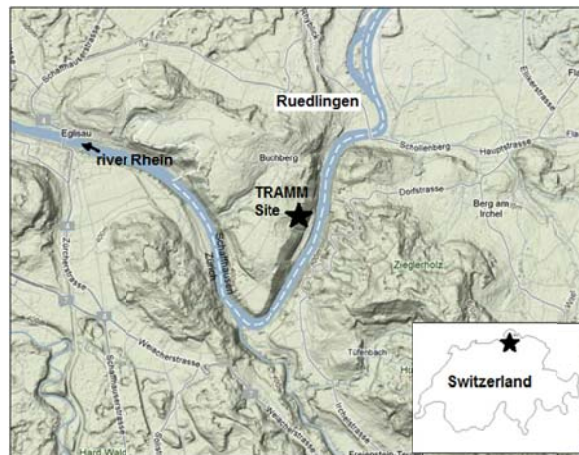

FIG. 1. The TRAMM test site in Ruedlingen, Switzerland.

Ruedlingen village was chosen following an extreme event in May 2002 in which 100 mm of rain had fallen in 40 minutes, leading to 42 landslides around the local area (Springman et al., 2010).
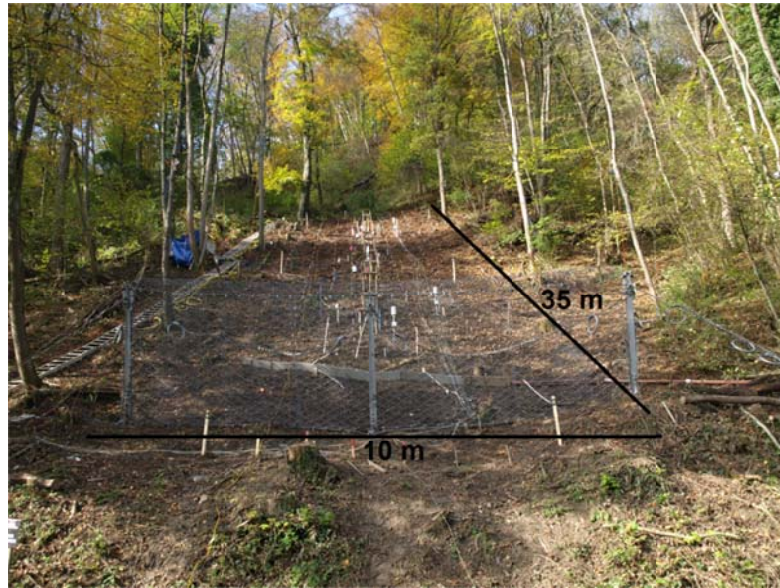
FIG. 2. The test site has a dimension of 10 m by 35 m.

THE RUEDLINGEN EXPERIMENT

After identification of a possible steep slope that would be susceptible to a shallow landslide on the basis of geology, topography, accessibility, vegetation and expected ground profile, the layers of soil and depth to rock was characterized to decide whether the experiment would be feasible or not. A series of test pits were dug around the edges of the projected test field to determine soil layering, investigate the root systems, locate rock depth and extract soil samples.

Photogrammetric Network Design

Two tall trees on the front side of the experiment area (shown as Tree1 and Tree2 in Fig. 3), both of which are approximately 25 meters in height, were selected to set up the cameras. A 4-camera arrangement (2 cameras per tree) was used for adequate photogrammetric coverage of the experiment area.
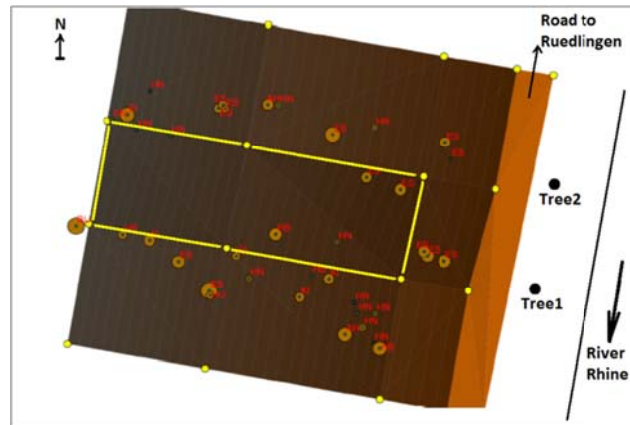
FIG. 3. The test site is delineated by yellow border lines. Tree1 and Tree2 are located on the opposite site of the road to Ruedlingen.

An initial map of the area (Fig. 3) was generated using the basic geodetic equipments. This information served as input to an in-house developed photogrammetric network simulation tool, called PanCam. The PanCam is a routine which can estimate the a posteriori point positioning precision numbers provided that the input parameters of the designed photogrammetric network are given (Amiri Parian et al., 2007). The proper camera formats and lenses were interactively examined in the simulation environment. The network design and simulation steps are essentially required in order to predict the theoretical precisions of point coordinates (Saadatseresht et al., 2004; Olague and Dunn, 2007; Rieke-Zapp et al., 2009).

The sprinkling experiment aims to trigger a shallow landslide where the slow mobilisation of the mass is followed by a sudden movement towards downhill. Therefore, a high speed camera set which has the continuous coverage (day and night) capability must be used. Accordingly, 1·3 Megapixel IDS uEye UI-6240 C (IDS - Imaging Development Systems GmbH, Germany) video cameras were chosen for the image acquisition (Fig. 4). Technical details of the cameras are given in Table 1. Intentionally, a CCD type of sensor is preferred over the CMOS sensors, since radiometric quality is a concern especially for the night time images.

FIG. 4. IDS uEye UI-6240 C Gigabit Ethernet video camera.

TABLE I. Technical details of IDS uEye UI-6240 C video cameras.

	IDS UI-6240 camera
Sensor type	CCD
Sensor size	½ inch
Image format	1280 × 1024 pixels
Shutter	Global shutter
Frame rate	14 fps
Pixel pitch	4·65 microns
Data transmission protocol	Gigabit Ethernet

Using the PanCam tool, a priori point positioning accuracy of the signalized targets was estimated to ± 12·4 mm in the horizontal direction and ± 4·2 mm in the vertical direction (Fig. 5). A priori standard deviation of the image point observations was assumed as ± 0·1 pixel. The design consideration for the project is to track the points during the landslide within a positional accuracy of ± 1–2 cm. According to the simulation results, the photogrammetric network, as designed, meets this requirement satisfactorily.
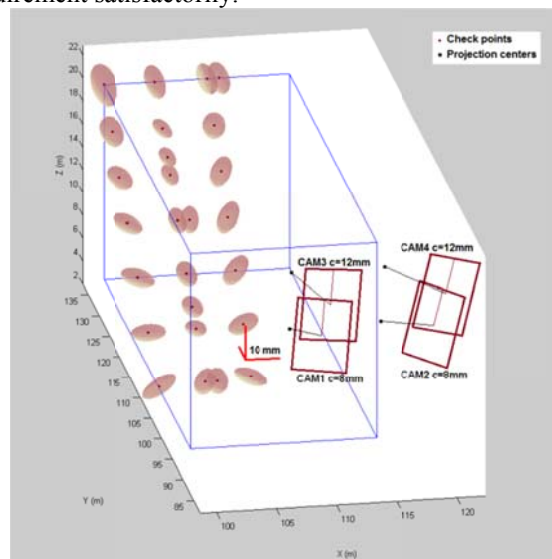

FIG. 5. The a priori estimated error ellipsoids of some representative signalized targets.

Equipments and Installation

The four IDS cameras were equipped with two 8·0 mm and two 12·0 mm C-mount lenses. The two 8·0 mm lenses equipped cameras (CAM1 and CAM2 in Fig. 6) were directed towards the bottom-side of the experiment area, and the other two cameras with 12·0 mm lenses (CAM3 and CAM4 in Fig. 6) were directed towards the upper-side of the experiment area. The two lower cameras

(CAM1 and CAM2) and the two upper cameras (CAM3 and CAM4) were 13 m and 18 m above the ground, respectively. The baseline of the cameras is 5·1 m along the trees, and 6·2 m across the trees. This arrangement gave 100% imaging overlap of all cameras.
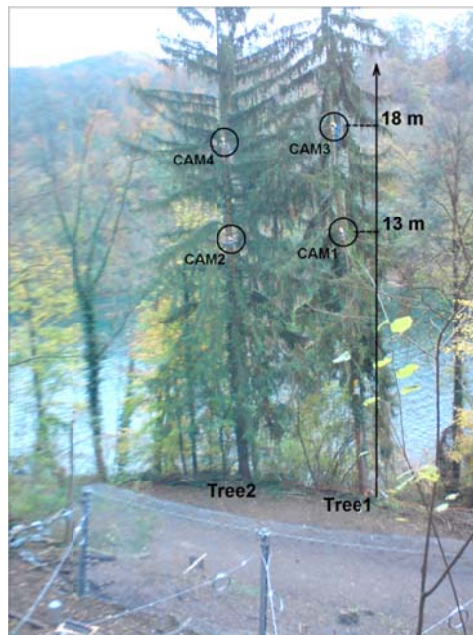

FIG. 6. The four cameras were fixed on two trees at 13 meters and 18 meters height, respectively.

The cameras were placed in housing shields (Fig. 7) which protect them against snow, rain, dust and other kind of environmental effects. They were fixed on the trees by a professional climber.

All cameras were connected to a central computer using approximately 100 m Cat-6 Ethernet cables. The control computer was a Fujitsi-Siemens Celsius W–360 PC with an Intel Core 2 Quad 2.4 GHz CPU, 4 GB DDR2 RAM, 1x 250 GB and 2x 500 GB 7200 rpm SATA II harddisks, and MS Windows Server 2003 R2 Enterprise operating system. An Intel Pro/1000 PT Quad Port Network Interface Card (NIC) was used for the Ethernet protocol communication.

The cameras were set to operate at 10 frames per second (fps) data acquisition rate. The imaging frequency of the four cameras was synchronized by an in-house developed image acquisition software, which is a MS Windows multi-threading application, developed using C# programming language and IDS SDK (Software Development Kit) library functions. The standard MS Windows software are single-threading applications, where the instructions are executed serially. The multi-threading is a software programming concept where multiple instructions can run synchronously in parallel. The in-house image acquisition software enables the four cameras to shoot (and to store) the frames simultaneously at the same instant. Our multi-threading software approach has a

synchronisation error of ±2 milliseconds in all cases. Alternative to the software synchronisation is the hardware synchronisation where the external triggers and additional synchronisation cables are employed. However, this approach brings additional cost to the project budget.

FIG. 7. The cameras placed in housing shields were fixed on the trees by a climber.

The synchronization of the cameras is extremely important when monitoring such dynamic events. Otherwise, we could have bought cheaper cameras with larger image format, and would thus have obtained even better results.

Deformations were monitored during the experiment, both on the surface via photogrammetric camera network and within the soil mass, using a flexible probe equipped with strain gauges at different points and two axis inclinometers on the top and acoustic sensors. Instruments were installed at depths of 15, 30, 60, 90, 120, and 150 cm below the ground surface over the slope, including jet-fill tensiometers, time domain reflectometers (TDRs), Decagon TDRs, piezometers, soil temperature sensors, deformation probes, earth pressure cells, acoustic sensors and rain gauges (Springman et al., 2010). A ring-net barrier (provided by Geobrugg AG) was set up at the foot of the slope to protect the road (Fig. 2 and 6).

Signalized Targets

76 yellow tennis balls (with 80 mm diameter), glued on 25–35 cm wooden sticks, were used as the artificial targets. The sticks were pushed vertically to the ground in a regular grid arrangement.

13 tennis balls were occluded by a textile strip (right side of Fig.9). The remaining 63 tennis balls were effectively used in the continuation of the experiment. The balls were appeared 5 to 7 pixels in diameter in the images.

12 well distributed ground control points (GCPs) were established on the surrounding stable trees. The 3D coordinates of the GCPs were measured with a Leica TCR407 Power reflectorless electronic theodolite with a standard deviation of ± 2·0 mm for the X, Y and ± 1·0 mm for the Z coordinates, respectively.

The GCPs and the balls were illuminated using strong halogen lamps during night time. The radiometric settings (brightness, contrast, gain and exposure time) of the cameras were altered periodically for the day time and night time by our in-house developed image acquisition software. The same software was also used for automatic shooting and storing the images.

Calibration and Orientation

A laboratory testfield calibration was performed on the cameras and their set up. The photogrammetric 3D calibration field at the Institute of Geodesy and Photogrammetry at ETH Zurich was used (Akca and Gruen, 2009). It is 3·4 m × 2·0 m × 1·0 m in size (Fig. 8). The room has stable temperature (22^0 C) and humidity (40%) by means of air conditioning. The 3D coordinates of 87 well distributed control points were measured using a Leica Axyz system. The average theoretical precision values of the control points are ±0·03 mm, ±0·05 mm and ±0·03 mm for the X, Y and Z axes, respectively. Note that the Y axis is the depth direction here.

Nine images were taken for each of the four cameras from three locations (each of which has three stations, down, middle and up) in a convergent geometry mode. Six images were taken in normal mode and the remaining three images were rotated in order to de-correlate the interior and exterior orientation parameters.

All tie point and control point measurements were carried out interactively using the least squares image matching method implemented in the BAAP software. The BAAP is a GUI based MS Windows software, and it was specifically designed for close range photogrammetric applications (Akca and Gruen, 2009). It was developed (in-house) using C++ Builder 5.0 integrated development environment (IDE).

FIG. 8. The photogrammetric 3D calibration field at the Institute of Geodesy and Photogrammetry at ETH Zurich. The picture was taken by CAM1.

The self-calibrating bundle adjustment, implemented in the SGAP software, was used for the final estimation of the parameters. The SGAP software has a command-line interface and offers sophisticated photogrammetric bundle adjustment modules. It has been developed at the Institute of Geodesy and Photogrammetry at ETH Zurich (Beyer, 1992).

The average of the standard deviation of image point observations $\hat{\sigma}_0$ is $0 \cdot 36$ microns, which translates to 1/13 of a pixel of the CCD sensors. Some parts of the results are given in Table 2. Columns *STD-X*, *STD-Y* and *STD-Z* give the average theoretical precision values of tie points for the respective cameras. The best relative precision of 1:22000 in-plane and $0 \cdot 0066\%$ of average depth was achieved for CAM1.

TABLE II. Results of the 3D testfield camera calibration.

Camera name	Camera constant	$\hat{\sigma}_0$	STD-X	STD-Y	STD-Z
	(mm)	(microns)	(mm)	(mm)	(mm)
CAM1	8·286 ±0·001	0·40	0·14	0·33	0·11
CAM2	8·296 ±0·001	0·35	0·14	0·36	0·12
CAM3	12·047 ±0·001	0·34	0·22	0·48	0·15
CAM4	12·075 ±0·001	0·34	0·19	0·33	0·13
Mean		0·36	0·17	0·38	0·13

STD-X : Average theoretical precision values of tie points along the X axis.

The estimated additional parameters (APs) are given in Table 3. In all cases, the remaining APs ($K2$ and $K3$ coefficients of the radial distortion, affinity, shear, $P1$ and $P2$ coefficients of tangential distortion) were excluded from the bundle adjustment due to statistical significance and determinability problems. The small values of the theoretical precisions and algebraic correlations (less than 0·41 in all cases) of APs indicate the stability of the computations.

TABLE III. Estimated additional parameters.

Camera name	x_0 (mm)		y_0 (mm)		$K1$	
CAM1	−0·026	±0·001	−0·155	±0·001	−8.775 E-004	±3.918 E-006
CAM2	0·079	±0·001	−0·175	±0·001	−8.772 E-004	±4.493 E-006
CAM3	0·040	±0·001	0·066	±0·001	−2.756 E-004	±3.695 E-006
CAM4	0·122	±0·001	0·098	±0·001	−1.896 E-004	±3.154 E-006

The estimated camera calibration parameters were considered as constant over time in the following point positioning computations. Since the camera stations on two tall trees were not stable platforms and were moving with the wind, the exterior orientations (EOs) of the cameras were calculated for each camera/image frame individually, by use of the GCPs.

The Landslide

Image acquisition of the second sprinkling experiment was started on 16.03.2009 at 3:28 pm and ended on 17.03.2009 at 11:58 am. The photogrammetric system worked continuously for 20 hours and 30 minutes, and collected approximately 2·5 million grey-level images of the scene (Fig.9). Although the cameras can provide 24–bit colour images, 8–bit grey scale images were acquired for faster data transmission and processing purposes.

With the properly aligned sprinklers, the rainfall was adjusted to an average distribution of 15 mm/h. Uniform sprinkling was achieved with 360^0 spray nozzles. Thanks to the high infiltration capacity, the fine mist penetrated into the soil quickly. Thus, any considerable surface runoff did not occur during the experiment.

There was an instant response in the upper part of the field as the saturation degree increased, suctions dropped and then the water table rose over 5 hours to about 1·5 m below ground level, where it stayed for the next 10 hours. 15 hours after the rainfall had begun, at 3:00 am, the upper right quadrant started to creep downslope, with the rate increasing until 3:23 am (Fig. 10, 11 and 12). It took 36 seconds to mobilize about 130 m^3 of soil and roots, which travelled on a slightly leftward trajectory towards the tree stump in the lower part of the field, which re-directed the flow to accelerate towards the bottom right, whereupon it took only 12 seconds more to impact on the protection net (Springman et al., 2010).

Post-processing, Target Tracking and Point Positioning

The images were processed in three temporal frequency groups:

1) *Hour-by-hour (1#fph)*: 1 frame per hour starting from 6:00 pm until 3:00 am, totally 8 epochs, and 8×4 = 32 images.

2) *Minute-by-minute (1#fpm)*: 1 frame per minute starting from 3:01 am until 3:23 am, totally 23 epochs, and 23×4 = 92 images.

3) *Original imaging frequency (5#fps)*: 5 frames per second starting from 3:23:00.000 am until 3:24:00.909 am, totally 263 epochs, and 263×4 = 1052 images.

The cameras were set to operate at 10 fps through the control software. However, the average image acquisition speed of 8 fps during the day time and 5 fps during the night time was able to be achieved. This deficiency was reported to IDS, but no satisfying explanation (and solution) could be given.

FIG. 9. An image taken from CAM3 in the evening at 6:00:00 pm. The smaller white spots are the ping-pong balls of the first experiment. The larger white ones are the tennis balls.

FIG. 10. A CAM3 image just before the landslide at 3:23:00 am.

FIG. 11. A CAM3 image just after the landslide at 3:24:18 am.

FIG. 12. A CAM3 image in the morning at 7:00:00 am.

All image measurements were performed automatically using an image tracking algorithm implemented as a module inside the BAAP software.

In an initialization step, the user measures the tennis balls semi-automatically of only the 6:00 pm images of the 1#fph group, using a cross-correlation template matching. The template image is white circle that is generated artificially on a black background, and is 11x11 pixels in size (Fig. 13). At this step, the initial positions of the targets are given by the operator. Then, the tracking algorithm automatically searches for the template image in the next frames, recursively. The 11x11 pixel cross-correlation window seeks the sub-pixel matching location inside a circular search area of 15 pixels in radius. The origin of the circular search area is defined by the pixel coordinates given in the previous frame. If the cross-correlation coefficient goes below of 0.85 for any point, this point is excluded to be tracked in the subsequent frames. Such points are lost mostly due to occlusions or jumping the balls away by the landslide.
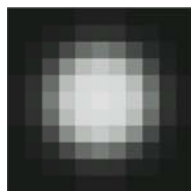

FIG. 13. The template image is 11×11 pixels in size.

The tracking algorithm produced satisfactory results. Only 4% of the resulting image measurements were erroneous. All erroneous cases occurred in 5#fps computations when the landslide had activated. Fig. 14 shows an example where point 33 has been lost in the last frame. The point was obscured by another object here. The tracking algorithm finds an erroneous location for point 33 whose cross-correlation coefficient is less than the threshold limit (0.85). This point was excluded in the following frames.
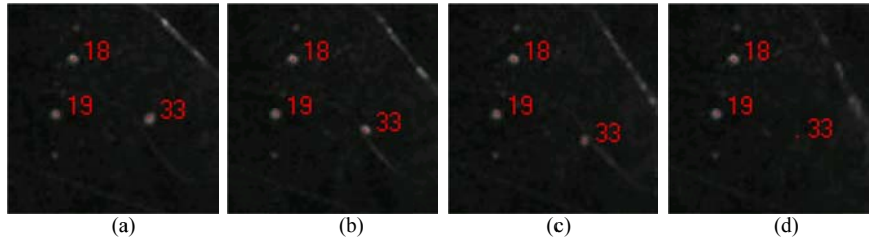

| (a) | (b) | (c) | (d) |

FIG. 14. Four consecutive frames of CAM1 during the landslide activity. The images are enlarged three times for the visualization purposes. The tennis ball 33 has been lost in the last frame.

Although the network configuration gave 100% imaging overlap for all four cameras, the field instruments, for example sprinklers, deformation probes, and acoustic sensors, obscured a few of the tennis balls. 8 of the total 63 tennis balls (13%) were visible in 3−fold images, the remaining 55 tennis balls (87%) were captured in 4−fold images.

As a result, $(8-1) + 23 + 263 = 293$ images (or epochs) were measured automatically. This procedure was repeated for image sets of the four cameras.

The image measurements generated (together with their ancillary data) were input into the SGAP software. The SGAP software computed 294 individual bundle adjustments in the batch computation mode. The average sigma naught of the all computations is 0·43 microns, which is equal to 1/11 of a pixel of the imaging system (Table 4). The mean theoretical precisions of the estimated coordinates of the tennis balls are ± 16·9 mm along the horizontal plane and ± 6·5 mm along the vertical direction The achieved precision numbers are in close agreement with the simulation results and the project requirements. Note that these numbers are 1−σ values which accounts for only 68% of the errors falling into this range. The relative precision values can be computed considering the size of the test site and average depth, which are 1:5000 in-plane and 0.03% of depth.

The computation took 26 minutes on a high-end desktop computer. In a typical bundle adjustment of 1#fph and 1#fpm computations where any tracking point has not been lost, the following structure is observed:

Data definition:
    Images: 4
    APs (fixed): 4
    Object points: 63
    GCPs (fixed): 10

Observations:
    Image point observations: 504
Unknowns:
    Object point coordinates: 189
    Exterior orientation parameters: 24
Degree of freedom: 291.

TABLE IV. Theoretical point positioning precisions of the tennis balls.

Groups	$\hat{\sigma}_0$	STD-X	STD-Y	STD-Z
	(microns)	(mm)	(mm)	(mm)
1#fph	0·45	7·0	15·5	6·6
1#fpm	0·43	7·0	15·4	6·5
5#fps	0·41	7·0	15·4	6·3
Mean	0·43	7·0	15·4	6·5

The outliers were automatically identified and localized with a two-level strategy:
1) The limit of the cross-correlation coefficient set as 0.85 in the tracking algorithm run by the BAAP software.
2) Outlier test in the batch mode bundle adjustments run by the SGAP software.

Once located, each outlier was inspected and corrected interactively.
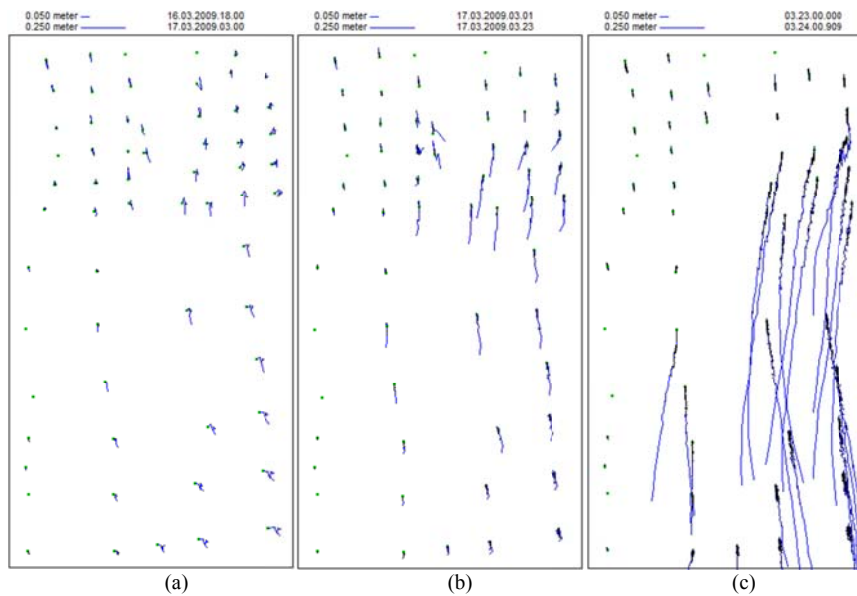

FIG. 15. Horizontal displacement of the tennis balls, (a) 1#fph between 6:00 pm and 3:00 am, (b) 1#fpm between 3:01 am and 3:23 am, and (c) 5#fps between 3:23:00 am and 3:24:00 am.
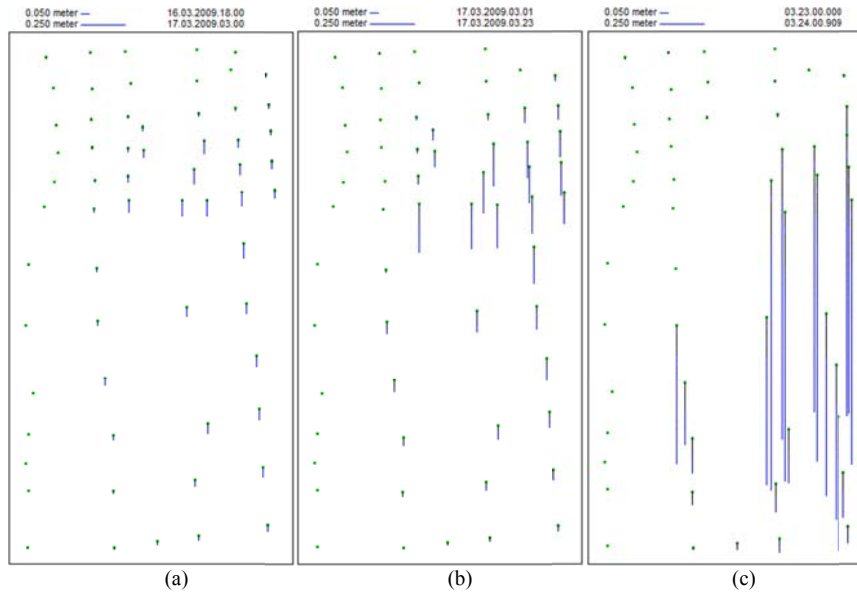
FIG. 16. Vertical displacement of the tennis balls in the same timeframes as Fig. 16, (a)1#fph, (b)1#fpm, and (c)5#fps.

The relative displacements along the horizontal and vertical directions were illustrated graphically in Fig. 15 and 16. The displacements were computed by subtracting the X-Y-Z coordinate values of the subsequent frames on a point basis. A similar comparison can also be performed in the surface domain (Gruen and Akca, 2005; Akca, 2010; Akca et al., 2010).

Starting from 6:00 pm till 3:00 am, the 1 frame per hour computations (1#fph) show relatively small planar movements both along the slope and across the slope directions (Fig. 15a).

At 9:00 pm the surface of the upper half of the area was raised 1 – 3 cm. This instant was the extreme upward location of the vertical movement of the surface. Between 9:00 pm and 1:00 am the vertical movement was gradually neutralised. In the next hour at 2:00 am the vertical movement suddenly changed its direction to downward starting to lowering 2 – 4 cm. At 3:00 am, the right half of the field was lowered by 4−6 cm (Fig. 16a). The slope has kept its steady state during 12 hour from starting the sprinkling at 3:00 pm to this moment.

Between 3:01 am and 3:23 am, the upper right quadrant started to move downslope in slow motion, at some points, totally 40 cm in the horizontal plane (Fig. 15b) and 30 cm in the vertical direction (Fig. 16b). The velocity is 3·0 cm/minutes on average and 11·8 cm/minutes at maximum.

The landslide occurred between 3:23 am and 3:24 am, lasting 48 seconds. In this time span, the upper right quadrant flowed along the slope with an average velocity of 14·0 cm/seconds, and a maximum speed of 100·4 cm/seconds was reached at some locations (Fig. 15c and 16c).

The wooden sticks of the tennis balls have a depth of 20−25 cm into the ground. They are used as targets and not for tracers on the surface that would represent debris particles in size or weight. The tennis balls are controlled by differential movements of 20−25 cm thick debris packages. The 3D movements are assumed to follow the landslide direction. Occasionally, 3D movements may point into any direction rather than downhill. Even size and installation of the wooden sticks would have influence on the observed movement. These small perturbations are minor and do not disturb the results significantly.

CONCLUSIONS

The Ruedlingen experiment is a sub-project within the framework of the TRAMM project. The express purpose is to trigger a rainfall induced landslide, having characterized the slope, and exposed it to continuous observation using high resolution cameras. A photogrammetric network was designed and installed. Photogrammetry is a cost-effective and accurate method for such tasks. In the experiment the photogrammetric monitoring system has a cost of CHF 13K including cameras, lenses, protection cases, NIC card and cables. The intellectual property of the developed software packages has to be considered separately.

Planning and designing are the key steps when environmental conditions and project specifications have strict limitations. The simulations, performed by the in-house developed PanCam routine, aided the design step. Different photogrammetric network options were simulated; the optimal one was chosen by considering the project requirements and the budget. In this way, just at the beginning of the project, the outputs of the final computations could be predicted and the hardware was purchased accordingly.

Based on the simulation results, 4 IDS cameras with 1280×1024 CCD sensors were used. Although the factory specifications of the IDS cameras report a 14 fps image acquisition rate, only a 5 to 8 fps acquisition rate was achieved during the experiments.

Nevertheless, results of the photogrammetric processing fulfilled the project requirements largely because the landslide developed over a long period of time than an earlier example in Japan (Ochiai et al., 2004) which had failed and flowed within about 5 seconds.

The surface deformation was quantified by tracking the small (tennis) balls pegged on the ground. The average 3D point-positioning precision of ±1.8 cm was achieved. The results of the photogrammetric work provide a better understanding of surface dynamics of landslides.

REFERENCES

AKCA, D., 2010. Co-registration of surfaces by 3D Least Squares matching. *Photogrammetric Engineering and Remote Sensing*, 76(3): 307–318.

AKCA, D., GRUEN, A., 2009. Comparative geometric and radiometric evaluation of mobile phone and still video cameras. *The Photogrammetric Record*, 24(127): 217–245.

AKCA, D., FREEMAN, M., SARGENT, I., GRUEN, A., 2010. Quality assessment of 3D building data. *The Photogrammetric Record*, 25(132): 339–355.

AKCA, D., GRUEN, A., ASKARINEJAD, A., SPRINGMAN, S.M., 2011. Photogrammetric monitoring of an artificially generated landslide. *The International Conference on GeoInformation for Disaster Management (Gi4DM'11)*, Antalya, Turkey. 10 pages (on CD-ROM).

AMIRI PARIAN, J., GRUEN, A., COZZANI, A., 2007. Monitoring of the reflectors of ESA's Planck telescope by close-range photogrammetry. *Journal of Applied Geodesy*, 1(3): 137–145.

ANGELI, M.-G., PASUTO, A., SILVANO, S., 2000. A critical review of landslide monitoring experiences. *Engineering Geology*, 55(3): 133–147.

ASKARINEJAD, A., CASINI, F., KIENZLER, P., TEYSSEIRE, P., SPRINGMAN, S.M., 2010. Mountain risks: two case histories of landslides induced by artificial rainfall on steep slopes. *International Conference on Mountain Risks: Bringing Science to Society*, Florence, Italy. 437 pages: 201–206.

AYALEW, L., YAMAGISHI, H., MARUI, H., KANNO, T., 2005. Landslides in Sado Island of Japan: Part I. Case studies, monitoring techniques and environmental considerations. *Engineering Geology*, 81(4): 419–431.

BALDI, P., CENNI, N., FABRIS, M., ZANUTTA, A., 2008. Kinematics of a landslide derived from archival photogrammetry and GPS data. *Geomorphology*, 102(3–4): 435–444.

BELL., R., PETSCHKO, H., RÖHRS, M., DIX, A., 2012. Assessment of landslides age, landslide persistence and human impact using airborne laser scanning digital terrain models. *Geografiska Annaler: Series A, Physical Geography*, 94(1): 135–156.

BEYER, H. A., 1992. *Geometric and radiometric analysis of a CCD-camera based photogrammetric close-range system*. Mitteilungen Nr. 51, Institute for Geodesy and Photogrammetry, ETH Zurich. 186 pages.

CHADWICK, J., DORSCH, S., GLENN, N., THACKRAY, G., SHILLING, K., 2005. Application of multi-temporal high-resolution imagery and GPS in a study of the motion of a canyon rim landslide. *ISPRS Journal of Photogrammetry and Remote Sensing*, 59(4): 212–221.

CORSINI, A., PASUTO, A., SOLDATI, M., ZANNONI, A., 2005. Field monitoring of the Corvara landslide (Dolomites, Italy) and its relevance for hazard assessment. *Geomorphology*, 66(1–4): 149–165.

DEBELLA-GILO, M., AND KÄÄB, A., 2012. Measurement of surface displacement and deformation of mass movements using least squares matching of repeat high resolution satellite and aerial images. *Remote Sensing*, 4(1): 43–67.

DEWEZ, T., NACHBAUR, A., MATHON, C., SEDAN, O., KOBAYASHI, H., RIVIERE, C., BERGER, F., DES GARETS, E., NOWAK, E., 2010. OFAI: 3D block tracking in a real-sized rockfall experiment on a weathered volcanic rocks slope of Tahiti, French Polynesia. *International Symposium on the Rock Slope Stability (RSS 2010)*, Paris, France. 13 pages: (on CD-ROM).

DEWITTE, O., JASSELETTE, J.-C., CORNET, Y., VAN DEN EECKHAUT, M., COLLIGNON, A., POESEN, J., DEMOULIN, A., 2008. Tracking landslide displacements by multi-temporal DTMs: A combined aerial stereophotogrammetric and LIDAR approach in western Belgium. *Engineering Geology*, 99(1–2): 11–22.

GRUEN, A., AKCA, D., 2005. Least squares 3D surface and curve matching. *ISPRS Journal of Photogrammetry and Remote Sensing*, 59(3): 151–174.

LODHI, M.A., 2011. Earthquake-induced landslide mapping in the western Himalayas using medium resolution ASTER imagery. *International Journal of Remote Sensing*, 32(19): 5331–5346.

MALET, J.-P., MAQUAIRE, O., CALAIS, E., 2002. The use of Global Positioning System techniques for the continuous monitoring of landslides: application to the Super-Sauze earthflow (Alpes-de-Haute-Provence, France). *Geomorphology*, 43(1–2): 33–54.

MARTHA, T.R., KERLE, N., JETTEN, V., VAN WESTEN, C.J., KUMAR, K.V., 2010. Landslide Volumetric Analysis Using Cartosat-1-Derived DEMs. *IEEE Geoscience and Remote Sensing*, 7(3): 582–586.

METTERNICHT, G., HURNI, L., GOGU, R., 2005. Remote sensing of landslides: An analysis of the potential contribution to geo-spatial systems for hazard assessment in mountainous environments. *Remote Sensing of Environment*, 98(2–3): 284–303.

MORA, P., BALDI, P., CASULA, G., FABRIS, M., GHIROTTI, M., MAZZINI, E., PESCI, A., 2003. Global Positioning Systems and digital photogrammetry for the monitoring of mass movements: application to the Ca' di Malta landslide (northern Apennines, Italy). *Engineering Geology*, 68(1–2): 103–121.

NIETHAMMER, U., JAMES, M.R., ROTHMUND, S., TRAVELLETTI, J., JOSWIG, M., 2012. UAV-based remote sensing of the Super-Sauze landslide: Evaluation and results. *Engineering Geology*, 128(1): 2–11.

OCHIAI, H., OKADA, Y., FURUYA, G., OKURA, Y., MATSUI, T., SAMMORI, T., TERAJIMA, T., SASSA, K., 2004. A fluidized landslide on a natural slope by artificial rainfall. *Landslides*, 1(3): 211–219.

OLAGUE, G., AND DUNN, E., 2007. Development of a practical photogrammetric network design using evolutionary computing. *The Photogrammetric Record*, 22(117): 22–38.

PESCI, A., TEZA, G., CASULA, G., LODDO, F., DE MARTINO, P., DOLCE, M., OBRIZZO, F., PINGUE, F., 2011. Multitemporal laser scanner-based observation of the Mt. Vesuvius crater: Characterization of overall geometry and recognition of landslide events. *ISPRS Journal of Photogrammetry and Remote Sensing*, 66(3): 327–336.

PETLEY, D.N., MANTOVANI, F., BULMER, M.H., ZANNONI, A., 2005. The use of surface monitoring data for the interpretation of landslide movement patterns. *Geomorphology*, 66(1–4): 133–147.

RIEKE-ZAPP, D.H., ROSENBAUER, R., SCHLUNEGGER, F., 2009. A photogrammetric surveying method for field applications. *The Photogrammetric Record*, 24(125): 5–22.

SAADATSERESHT, M., FRASER, C.S., SAMADZADEGAN, F., AZIZI, A., 2004. Visibility analysis in vision metrology network design. *The Photogrammetric Record*, 19(107): 219–236.

SPRINGMAN, S., ASKARINEJAD, A., KIENZLER, P., CASINI F., SPERL, M., BLEIKER, E., AKCA, D., GRUEN, A., 2010. The Ruedlingen monitoring and landslide experiment. *D-BAUG Annual Report 2009*, Department of Civil, Environmental and Geomatic Engineering, ETH Zurich, 84 pages: 26–31. http://www.baug.ethz.ch/about/annual_reports/baug_report_2009.pdf [Accessed: 20th April 2012].

TARCHI, D., CASAGLI, N., FANTI, R., LEVA, D.D., LUZI, G., PASUTA, A., PIERACCINI, M., SILVANO, S., 2003. Landslide monitoring by using ground-based SAR interferometry: an example of application to the Tessina landslide in Italy. *Engineering Geology*, 68(1–2): 15–30.

TRAVELLETTI, J., OPPIKOFER, T., DELACOURT, C., MALET, J.-P., JABOYEDOFF, M., 2008. Monitoring landslide displacements during a controlled rain experiment using a long-range terrestrial laser scanning (TLS). *The International Archives of the Photogrammetry, Remote Sensing and Spatial Information Sciences*, 37(B5): 485–490.

Résumé

Zusammenfassung